PREDICTIVE QSAR MODELING OF COMPOUNDS INHIBITING CYTOCHROME
P450 3A4-MEDIATED METABOLISM OF TESTOSTERONE AND 7-BENZYLOXY-
4-TRIFLUOROMETHYLCOUMARIN

By

CHRISTOPHER MAYER-BACON

A thesis submitted to the

Graduate School-Camden

Rutgers, The State University of New Jersey

In partial fulfillment of the requirements

For the degree of

Master of Science

Graduate Program in Computational and Integrative Biology

Written under the direction of

Dr. Hao Zhu

and approved by

———————————————

Joseph Martin

———————————————

Grace Brannigan

———————————————

Hao Zhu

January 2014

ABSTRACT OF THE THESIS

PREDICTIVE QSAR MODELING OF COMPOUNDS INHIBITING CYTOCHROME P450 3A4-MEDIATED METABOLISM OF TESTOSTERONE AND 7-BENZYLOXY-4-TRIFLUOROMETHYLCOUMARIN

By: CHRISTOPHER MAYER-BACON

Thesis Director:

Hao Zhu

Enzymes in the cytochrome P450 family are responsible for much of the first-pass metabolism of xenobiotic compounds. Within this family, the hepatic 3A4 isoform (CYP3A4) is responsible for the first-pass metabolism of over half of the drug compounds currently on the market. This substrate promiscuity increases the risk of dangerous drug-drug interactions (DDIs), in which a drug compound inhibits the metabolism of other compounds by CYP3A4, leading to drug inactivity or the accumulation of the non-metabolized drug in the body. These risks have led to numerous quantitative structure-activity relationship (QSAR) and SAR studies of CYP3A4 inhibitors to determine the structural characteristics common to inhibitor compounds. Evidence of multiple binding pockets necessitates the use of a variety of probe substrates, resulting in different. From the published literature and patents, we collected compounds with inhibition data against CYP3A4, using either 7-benzyloxy-4-trifluoromethylcoumarin (BFC) or testosterone (TST) as the probe substrate and measuring inhibition as $-\log_{10}(IC_{50})$ (pIC$_{50}$). We then developed QSAR models using

two descriptor selection methods (random forest and genetic algorithm-k nearest

neighbors (GA-kNN) and two descriptor sets (MOE and Dragon). The resulting eight

models were validated via five-fold cross validation and external validation. While the

cross-validation results are good for all models, most models had low external

predictivity. By analyzing the models with the best external predictivity (those using

Dragon descriptors and GA-kNN descriptor selection), we found several atom-type and

P-VSA-like descriptors that showed a sizable difference in importance between the

models from the BFC and TST data. These descriptors reflect studies from prior QSAR

studies on characteristics of CYP3A4 inhibitors. Results from this study could be used to

account for differences in *in vitro* inhibition screens using multiple probe substrates.

ACKNOWLEDGEMENT

First, I would like to thank my advisor and mentor Dr. Hao Zhu. His classes introduced me to computational chemistry and his guidance helped me improve my writing and planning for future projects. The skills and tools he gave me have opened up numerous possibilities for my studies beyond Rutgers-Camden.

In the Zhu lab, I'd like to thank David Zhang for help with developing and troubleshooting many of the programs used in this research. I'd also like to thank Marlene Kim for her explanations of experimental procedures that were still new to me. Having her nearby was always useful when I needed a second opinion on my findings or ideas. Thanks also to the other members of the Zhu lab (Abena Boison, Dan Russo, and Brienne Sprague) for providing feedback and advice on my various drafts.

Thanks to Margaret-Ellen Johnson at Drexel, who helped critique my manuscript drafts and gave some much-needed advice for presenting my research.

TABLE OF CONTENTS

LIST OF FIGURES

Introduction

Among various hepatic enzymes that are involved in the first-pass metabolism, cytochrome P450 enzymes (CYPs) are the most prevalent. CYPs are a diverse family of hepatic heme-thiolate proteins with 57 known human *CYP* genes [1] and are responsible for most of the first-pass metabolism of drug compounds in humans. Roughly 75% of all marketed drugs are metabolized by CYPs [2]. One CYP isoform, CYP3A4, plays a critical role in this process by metabolizing 50-60% of those drugs[2]. Like many other CYP enzymes, CYP3A4 binds molecular oxygen to its heme iron, forming an activated iron-oxygen intermediate. This intermediate can then perform several reactions with substrate molecules, including alkyl carbon hydroxylation, O- and N-dealkylations, and aromatic ring hydroxylation[3]. With an active site as large as 1,386 Å^3 [4], CYP3A4 can accommodate substrates of various sizes, including macrolide antibiotics like cyclosporine. When an enzyme is actively metabolizing various compounds, the potential for DDIs induced by relevant inhibitors must be considered. An inhibitor of CYP3A4 metabolism could inhibit bioactivation of prodrugs or prevent drug's' metabolism and clearance, leading to potential side effects. To prevent DDIs induced by the CYP3A4 inhibitors, screening potential drug compounds for their CYP3A4 inhibitions has become a standard practice in drug discovery.

Along with metabolizing large substrate molecules such as cyclosporine and bromocriptine, CYP3A4 also displays non-Michaelis Menten kinetics[5] due to binding with multiple substrate molecules simultaneously. Lu et al. measured the CYP3A4 metabolism rates of different substrates, such as testosterone, 7-benzyloxy-4-trifluoromethylcoumarin (BFC), and 7-benzyloxyquinolone. The results showed little or

no competition between any two substrates. Thus, this study suggests three different substrate binding domains in the CYP3A4 active site[6]. Galetin, Clarke and Houston performed a similar kinetic interaction study using midazolam, testosterone, and nifedipine, in which represented different CYP3A4 substrate groups. This study confirmed the results from Lu et al. and also suggested one substrate binding domain acting as an effector site[5]. Domanski et al. studied site-directed phenylalanine/tryptophan mutagenesis of CYP3A4. By evaluating the mutant CYP3A4 metabolism of progesterone, testosterone, BFC and α-naphtoflavone, the team also confirmed an active pocket with three distinct binding sites[7].

The existence of multiple binding sites results in the different effects of an inhibitor on different substrates. Schrag and Wienkers observed such an effect in studying the inhibition of testosterone and triazolam metabolism by a variety of inhibitors. They found that some flavonoids (flavanone, flavone, and 3- and 6-hydroxyflavone), which were obtained from grapefruit juice, inhibited testosterone metabolism but enhanced the metabolism of triazolam[8]. Similar results were obtained by Shimada et al. In this recent study, flavone and flavanone were found to inhibit the formation of 4-hydroxymidazolam but enhanced the 1'-hydroxylation of midazolam by CYP3A4[9].

Common CYP3A4 substrates tend to be large, neutral, lipophilic compounds[10]. The preference for lipophilic substrates is reflected in QSAR studies of CYP3A4 inhibitors, where descriptors relating to lipophilicity abound. Ekins et al. studied the inhibition of CYP3A4-mediated midazolam 1-hydroxylation by 14 compounds, using 3D- and 4D-QSAR along with pharmacophore modeling, and developed computational

models for inhibitors of cyclosporine A metabolism and quinine hydroxylation based on prior published inhibition data. The correlations between experimental and predicted $K_{i(apparent)}$ values of models trained on the data sets from Ekins et al. and cyclosporine A metabolism inhibition are good (correlation coefficient of 0.77 for cyclosporine A data, 0.92 for Ekins et al. data) when tested against an external set of 8 compounds. Pharmacophore models trained on the quinine hydroxylation inhibition data were good as well, with a self-correlation of 0.92. These models all had at least one hydrophobic region, with models built with Ekins et al. and cyclosporine A metabolism inhibition data each containing three hydrophobic regions; overlap among the models showed two hydrophobic regions separated by hydrogen bond acceptors[11]. A structure-activity relationship (SAR) study by Row et al. seems to lend weight to the pharmacophore model proposed by Ekins et al. The Row et al. study compared the inhibitory potency of several furanocoumarin derivatives against testosterone metabolism, and found that the addition of an alkyl chain gives increased inhibitory potency, and shows a good fit with the hydrophobic region in the Ekins et al. pharmacophore model[12].

To date, several QSAR studies using different modeling methods and probe substrates have shown lipophilicity to play an important role in determining a compound's inhibition of CYP3A4 activity. Kriegl et al. used a partial least-squares discriminant analysis (PLS-DA) classification method to develop classification models of 930 compounds (551 in the training set, 379 in the test set) for the inhibition of erythromycin metabolism. The best model, with a squared external correlation between predicted and experimental activities (Q^2_{ext}) of 0.6, showed an inverse correlation between a compound's IC_{50} value and the number of aryl groups, as well as the

compound's logP[13].   Roy et al. made a similar finding after developing QSAR models for 28 compounds' inhibition on erythromycin metabolism. Using 5 different modeling methods, logP appeared as an important descriptor in all 5 models. Their best model, a genetic partial least-squares model with a modified r^2 ($r_{m(test)}^2$) of 0.581, predicted that effective inhibitors would have a logP value below 3.73[14]. Riley et al., by developing a generalized QSAR model for 30 compounds' inhibition of erythromycin metabolism, came to a similar conclusion. The inhibition potentials of these 30 compounds were positively correlated with their lipophilicity (measured as $logD_{7.4}$)[15]. Zuegge et al. developed a linear PLS classification model for inhibitors of BFC metabolism, based on a training set of 311 compounds. The model correctly classified 95% of the training set and 90% of a semi-independent test set (compounds culled from the raw dataset (1,152 compounds) that were not used in modeling). Among the five most relevant descriptors for the model, three descriptors measured the number of aromatic atoms, bonds, and rings. Additionally, the second principal component correlates with several descriptors that address lipophilicity (AlogP, number of aromatic bonds and rings, and paired lipophilic moieties[16]. A more recent, larger QSAR study by Sun et al. screened 13,538 compounds (6800 training, 6738 test) for inhibition of CYP3A4 metabolism of luciferase-based substrates, and then developed a support vector machine (SVM) model to classify compounds as active or inactive. In the optimized model, with a predictive accuracy of 0.87, compound active rate was correlated with the number of aromatic rings and molecular weight[10].

In addition to lipophilicity, the presence of heteroatoms and heterocyclic moieties, in particular nitrogen-containing rings, has been found to contribute to CYP3A4

inhibition. X-ray structures of CYP3A4 with ketoconazole, a potent CYP3A4 inhibitor, show a complex between the heme iron and the nitrogen atom in ketoconazole's imidazole group[17]. Several QSAR studies also demonstrated the importance of heteroatoms in their models. The Zuegge et al. study not only found aromaticity and lipophilicity to be important inhibitor characteristics, it also found the total number of hetero and aromatic atoms to be a highly relevant descriptor. In the Riley et al. study, compounds with a sterically unhindered N-heterocycle had IC_{50}'s roughly one order of magnitude lower than compounds lacking such a group. A study by Mao et al. developed pharmacophore models of the inhibition of CYP3A4 metabolism of four probe substrates. Through genetic algorithm (GA)-driven descriptor selection, the resulting model showed that imidazole, nitrile, and sulfonamide groups were common to inhibitors of BFC metabolism[18].

In previous studies, normally one individual modeling approach combined with one type of descriptors was applied to one CYP3A4 inhibitor set. Furthermore, although the complexities of the CYP3A4 active site were considered, there were few studies performed to compare the different outcomes of the models for the inhibition effects of same inhibitors on various substrates of CYP3A4. In this study, we constructed combinatorial QSAR (combi-QSAR) models for the inhibitors of CYP3A4 metabolism of two substrates, BFC and testosterone (Figure 1). Using the combination of two modeling approaches (k-nearest neighbor (kNN) and random forest (RF)) and two types of descriptors (Dragon and MOE), we successfully developed four different QSAR models for CYP3A4 BFC and testosterone inhibitors. Based on the modeling results, we compared the important chemical characteristics that contribute to the inhibition of BFC

metabolism and testosterone metabolism by CYP3A4. Moreover, we used our resulting

models to predict a set of new compounds after the models were developed.

Methodology

Data collection and curation

All data was collected from 31 papers and patents (in appendix), containing results of inhibition assays of CYP3A4. All studies reported the IC_{50} values of the test compounds, and employed either testosterone (TST) or BFC as the probe substrate. All IC_{50} values used for modeling were in μM and converted to $-\log_{10}(IC_{50})$ (pIC_{50}) to reduce the range of values. The SMILES structures of the compounds were screened with CaseUltra to remove stereochemistry and duplicate structures; this left 153 compounds with inhibition data against TST, and 120 compounds with inhibition data against BFC (hereafter called the TST set and BFC set, respectively), along with 22 compounds shared between the BFC and TST sets. Scatterplots of the shared compounds' pIC_{50} values for TST and BFC inhibition show a slight correlation between activities (R_0^2=0.53) (Figure 2), suggesting that there are some basic structural features common to inhibitors of both TST 6β-hydroxylation and BFC O-debenzylation. Figure 3 outlines the procedure we followed in developing and testing our models.

Eliminating duplicate activities

There were some instances of duplicate activities for a single compound. In such cases, we followed the flowchart in Figure 4. Where compounds were in the TST dataset or in the BFC dataset but not mentioned by Stresser et al.[19], we compared the pIC_{50} values from the various source studies, as well as the mean of those values. For activities within 0.1 log units of at least two other activities for the compound, we used that pIC_{50}

value in building the models. Otherwise, we did not include the compound in our models.

Descriptor generation

For both datasets, we generated 2D descriptors using MOE (version 2011) (186 descriptors) and Dragon (version 6) (4885 descriptors), giving a total of 4 datasets (TST-MOE, TST-Dragon, BFC-MOE, BFC-Dragon). MOE descriptors include physical properties (log P, molecular weight, molar refractivity, etc.), structural keys, E-state indices, and topological indices. Dragon contains descriptors for E-state values and counts, constitutional and topological attributes, walk and path counts, connectivity and information indices, 2D autocorrelations, Burden eigenvalues, molecular properties (e.g. logP), Kappa, hydrogen bond donor/acceptor counts, molecular fragment counts, and a variety of chemical fingerprints. Each dataset was then normalized, removing descriptors with a correlation > 0.9 between descriptors and a variance < 0.001 in the values of any one descriptor. After normalization, we had 97 descriptors in the TST-MOE dataset, 102 in the BFC-MOE dataset, 742 in the TST-Dragon dataset, and 802 in the BFC-Dragon dataset.

Modeling

Modeling was conducted for each dataset, using genetic algorithm k-nearest neighbors (GA-kNN) and random forest (RF) descriptor selection methods. Developed models were tested via 5-fold cross-validation.

GA-kNN

The kNN QSAR method[20] employs the kNN classification principle and the variable selection procedure. Briefly, a subset of nvar (number of selected variables) descriptors is selected randomly at the onset of the calculations. The nvar is set to different values, and the training set models are developed with leave-one-out cross-validation, where each compound is eliminated from the training set and its pIC_{50} is predicted as the average activity of k most similar molecules where the value of k is optimized as well (k = 1−9). The similarity is characterized by Euclidean distance between compounds in multidimensional descriptor space. A genetic algorithm is used to optimize the selection of variables. The objective of this method is to obtain the best leave-one-out cross-validated (LOO-CV) correlation possible by optimizing the nvar and k. Each kNN model is composed of several linear regression models, each of which contains some combination of descriptors that yields a model passing set thresholds. Additional details can be found in Zheng and Tropsha[20].

A genetic algorithm (GA) is designed to mimic biological processes of mutation and natural selection. It starts with a pool of randomly selected descriptor sets, and creates regression models from these sets. Some proportion of regression models will contain descriptors correlated with the desired endpoint. Among the group of well-correlated models, each can be modified through combination with other models in the group (breeding), or through the replacement of one descriptor with a randomly chosen alternative (mutation). Models are then reassessed and modified again, for a set number of cycles or until the models converge on a solution. More detailed information on genetic algorithms can be found in Goldberg[28].

Following our general QSAR modeling workflow methodology[21], all of the kNN

models were extensively validated. The modeling compounds were divided multiple

times into training/test sets using the Sphere Exclusion approach[22]. The statistical

significance of the models was characterized with R^2 for the training sets and LOO q^2 for

the test sets. The model acceptability cutoff values of the LOO-CV accuracy of the

validated and non-validated models (R^2 and q^2) were both set at 0.5. Models that did not

meet both training and test set cutoff criteria were discarded. The discussion of the

workflow used to develop validated QSAR models is given in a recent review[21].

The kNN program used the nearest 1-9 neighbors to a specific compound. The

descriptor range was between 5 and 50, scanning in steps of 5 descriptors to reduce

modeling time. Models had to clear a threshold of 0.5 for both R^2 and LOO q^2. These

thresholds ensured a wide variety of models would be produced for each dataset. The

rest of the GA-kNN modeling parameters are in Table 1.

Random forest

In machine learning, a RF is a predictor that consists of many decision trees and

outputs the prediction that combines outputs from individual trees. The algorithm for

inducing a random forest was developed by Breiman and Cutler[23]. In this study, the

implementation of the random forest algorithm available in R.2.15.1[28] was used. In the

RF modeling procedure, n samples are randomly drawn from the original data. These

samples were used to construct n training sets and to build n trees. For each node of the

tree, m variables were randomly chosen from the all of the available chemical

descriptors. The best data split was calculated using the m variables for the modeling set.

In this study, only the defined parameters (n = 500 and m = 13) were used for model development.

Testing against an external set

Using the PubChem BioAssay database, we collected compounds that had been screened for CYP3A4 inhibition of TST or BFC metabolism, only using assays that reported IC_{50} values. We sorted these compounds by the probe substrate used, and then removed stereochemistry and any duplicates in the respective training dataset. Descriptor generation and normalization were the same as in the original datasets, yielding 4 external datasets complementing the 4 model training datasets.

RF and GA-kNN models were constructed using the whole TST or BFC modeling set, under the same parameters as the modeling for the 5-fold split. These models were then used to predict the activities of the external compounds.

Descriptor analyses from GA-kNN and RF models

Scripts in R.2.15.1 and Perl were used with the RF and GA-kNN models, respectively, to determine the contribution of each descriptor to the developed model. The R script determined the importance of each variable in the model (based on the descriptor's position within the decision trees), while the Perl script counted the occurrence of each descriptor in the kNN models for each dataset, as a proxy measurement for descriptor importance.

Applicability Domain (AD)

While QSAR models can predict activities of any compound for which chemical descriptors can be computed, reliable predictions are unlikely if the model is tasked with predicting compounds dissimilar from those in the modeling set. The concept of AD is

used to avoid this scenario. In this paper, the applicability domain (D_T) was defined by the following equation:

$$D_T = \bar{y} + Z\sigma$$

Here, $\bar{y}$ is the average Euclidean distance squared between each compound in the external set and its k nearest neighbors in the training set (in this paper, we set $k=1$). σ represents the standard deviation of these distances, and Z is a parameter to control the significance level; increasing the value of Z increases the allowed distance threshold and potentially encompasses more compounds in the AD. For this study, we varied Z from 0 to 1 for each of the models developed. We opted to look at a range of applicability domains, as opposed to two or three AD sizes, in order to get a more complete picture of each model's performance. Figure 10 shows the resulting R^2 and MAE measurements for each model. Since ADs varied by both descriptor set and probe substrate set, the graphs are broken down according to those conditions.

Results and discussion

Database Overview

From the available literature and patents, we compiled two databases, both containing inhibition data against CYP3A4 in the form of pIC50. The databases differed in the probe substrates used in the assay; the BFC database used 7-BFC as the probe substrate to test inhibitory potency, while the TST database used testosterone instead. A single-factor ANOVA test of the activity distributions in the BFC (n=120) and TST (n=153) databases shows a statistically insignificant difference in the mean activity values (F=0.84, P=0.35). This suggests that the activity distributions (Figure 5) of the databases are unlikely to skew the modeling results.

Applicability domains for external sets

Since our training and test datasets are structurally diverse, using an applicability domain on our test set ensured that we would be predicting compounds with similar structural features as our training set. Figure 10 shows the coverage for the various z-values in the applicability domain measurements, and the R^2 and mean absolute error (MAE) measurements after plotting the predicted vs. actual activities of those test compounds within the applicability domain.

For both TST and BFC test sets, Dragon descriptors generally yielded greater R^2 values and lower MAE values than MOE descriptors at the same z-value. This could be due to the greater structural detail provided by the number of Dragon descriptors; this could also explain the lower coverage in BFC and TST test sets with Dragon descriptors

compared to MOE descriptors. Coverage of the external set remained low for the TST models (between 32-35% over most values of z). However, at similar coverage levels in the BFC test sets, performance was much poorer. This suggests that the TST external set contained a greater number of compounds that were highly similar to those in the corresponding training set.

In the BFC test set, both the RF and kNN models yielded poor external predictions with MOE descriptors; MAE values are greater than R^2 values over all applicability domains. With Dragon descriptors, the kNN model yielded fairly accurate predictions with applicability domains where z ≤0.4. Above that z-value, MAE increases drastically and R^2 falls.

In the TST test set the AD coverage for Dragon and MOE models (and by extension the R^2 and MAE values for the models) stayed constant over most of the z-value range. In the AD for the MOE models, the size of the AD stayed constant from z=0 to z=0.7. From z=0.8 and up, R^2 values for the RF and kNN models dropped below MAE for both modeling methods. For the Dragon models, the AD was much more stable. From z=0 to z=0.1, coverage increased slightly but with little effect on the R^2 or MAE of the models. From z=0.1 to z=1, there was no increase in the AD.

Model characteristics

Figure 6 shows the R^2 values for the generated models in the internal 5-fold cross-validation. Cross-validation statistics showed a greater R^2 correlation coefficient in models trained on the BFC database than those models trained on the TST database (R^2=0.62-0.72 for BFC, R^2=0.37-0.61 for TST), whereas the mean absolute error (MAE)

appears to be lower in the TST models than the BFC models (MAE=0.69-0.9 (mean=0.78) for BFC, MAE=0.57-0.8 (mean=0.64) for TST). Comparing modeling methods for both BFC and TST databases, random forest models had greater R^2 values and lower MAE values compared to kNN models. Models using Dragon descriptors consistently showed increased R^2 values and reduced MAE values when compared to the corresponding models using MOE descriptors. For both TST and BFC models, the consensus predictions performed better than the individual models, with the highest R^2 values and lowest MAE values (consensus BFC: R^2=0.72, MAE=0.65; consensus TST: R^2=0.61, MAE=0.55). To test the significance of the improvement of the consensus prediction over the individual models' predictions, single-factor ANOVA tests were conducted for the R^2 and MAE values of the BFC and TST models, all with α=0.05. There appeared to be no significant difference in R^2 values among the models from both the TST and BFC databases (TST: F=0.6, P=0.69; BFC: F=0.06, P=0.99), but the models from the TST database showed a significant difference in MAE values (F=6.45, P<0.05) with the kNN-Dragon model having the lowest MAE. No such difference was seen in the MAE values for the BFC models (F=0.82, P=0.50).

Structure-assay analysis

When using our models to predict our test compounds' activities, performance was markedly lower than in cross-validation (compare R^2 and MAE values for corresponding models between Figure 6 and Figure 10). While this could be due to several test compounds being outside of the AD of the training sets, we considered that the issue might be with the test compounds' structural neighbors in the training sets. Specifically, the training compounds most similar to the test compounds might have

performed differently in other CYP inhibition assays than the test compounds. If this were the case, the discrepancy in assay results could account for the incorrect predictions in our models.

We first converted all continuous pIC_{50} values (both experimental and predicted) to a binary format: 0 (inactive) if the activity was less than 0, and 1 (active) if the activity was 0 or greater. Using BFC and TST consensus predictions, we first determined which test compounds were predicted incorrectly. For each of those compounds, we determined the nearest structural neighbor(s) in the corresponding training set, using Dragon descriptors and a maximum z-cutoff of 2.05. For those test compounds with at least one training compound within the z-cutoff range, we used an in-house Perl script to obtain PubChem Bioassay ID numbers and outcomes for compounds in the BFC and TST training and test sets, using assays that tested 5 or more compounds. From those assays, we looked at those that turned up in corresponding training and test sets to identify CYP inhibition assays.

For the BFC training and test sets, we identified four shared assays measuring CYP inhibition, two of which were specifically for CYP3A4 inhibition. In the BFC test set (n=156), 73 binary predictions were incorrect. Of that number, 11 compounds had no close structural neighbor in the training set, effectively putting them outside of the model's AD. Thirty-four compounds differed from their training set neighbors in the outcomes of at least one CYP inhibition assay, suggesting that incorrect predictions for those test compounds could be due to different assay outcomes in their neighbors in the training set.

Interestingly for the TST test set, we found no shared assays between the training and test set, for CYP inhibition or otherwise. This is likely due to the parameters chosen for the assay search, specifically the number of compounds tested; while lowering the number of compounds per assay could garner more assays, it's unlikely that any of those assays would contain compounds from both training and test sets.

Descriptor analysis

For the mechanism analysis, we used the kNN-Dragon models of the BFC and TST databases, analyzing the frequency of descriptors in each model then comparing descriptor frequencies between models. Dragon descriptors contain more diverse sub-structure features compared to MOE descriptors, and the R^2 values for the kNN models exceeded those of the corresponding RF models, for both the BFC and TST databases.

Figure 7 shows the frequency of all descriptors used over both BFC and TST models. In the frequency comparison, we decided to analyze descriptors with a combined frequency of 30% or greater. This cutoff ensured that the number of descriptors would not be too extensive, and that the descriptors with high frequency in one or both of the models would be included in the analysis.

Figure 8 shows the difference in descriptor frequencies between the BFC and TST models. Several of the descriptors shown are atom-type descriptors specifying carbons one to two bond lengths away from highly electronegative heteroatoms. Two atom type descriptors, H-048 and H-049, show high relative frequency in the BFC and TST models, respectively. Both descriptors characterize the hydrogen of a CH group, with the carbon bonded to varying numbers of heteroatoms in a variety of hybridizations[24]. The two

descriptors differ in the number of heteroatom bonds present; CH groups under the H-049 descriptor possess more heteroatom bonds than those CH groups under the H-048 descriptor. In Figure 8, H-049 is seen to appear only in the TST model and H-048 appears more often in the BFC model.

Single-factor ANOVA analysis was performed on the values of the descriptors listed in Figure 8, comparing the TST and BFC databases for significant differences in the mean values of the descriptors. Table 2 reveals that both H-048 and 049 atom counts are significantly greater in the TST database (H-048: $F=7.48$, $p<0.01$; H-049: $F=28.19$, $p<0.01$). This suggests that the frequency of H-049 in the TST models might be due to the descriptor's increased frequency in the training compounds, while the increased frequency of H-048 in the BFC model likely results from an outsize contribution of that descriptor to the model's predictions.

Another pair of atom type descriptors, C-033 and C-042, characterizes carbon atoms with one single bond and one aromatic single bond; a C-033 atom shares an aromatic single bond with a heteroatom, while a C-042 atom shares both a single and aromatic single bond with heteroatoms. The C-033 descriptor is more frequent in the BFC model, while the C-042 descriptor is more frequent in the TST model. Table 2 shows counts of both descriptors to be significantly greater in the TST database (C-033: $F=21.04$, $p<0.01$; C-042: $F=9.47$, $p<0.01$). The significant differences in descriptor counts and frequencies in the two models suggest that the increased frequency of the C-033 descriptor in the BFC model is not a result of that descriptor's abundance in the training set, unlike the frequency of the C-042 descriptor in the TST model. Both of the atom type descriptors mentioned above, C-033 and H-048, are characterized by aliphatic

and aromatic bonds to heteroatoms. Prior QSAR studies of CYP3A4 inhibition[16,18] have found heteroatoms and aromatic heterocycles to be strong contributors to a compound's inhibitory activity against CYP3A4. Additional SAR studies have found that heterocycles such as furans[25] and unhindered N-heterocycles[15] lead to a substantial increase in CYP3A4 inhibition. Fitting with these prior findings, C-033 atom types are more prevalent in strong inhibitors from our BFC database.

Two other descriptors, P_VSA_LogP_6 and P_VSA_v_3, are concerned with the amount of a molecule's surface area with properties (in this case LogP and volume) in a specific range[26]. P_VSA_LogP_6 (the total surface area with a calculated LogP between 0.25 and 0.5) shows a relatively high frequency in the BFC model and no significant difference in the mean values in the BFC and TST databases ($F=1.79$, $p=0.18$). P_VSA_v_3 also shows a high frequency in the BFC model, but its mean value is also significantly greater in the BFC database ($F=4.37$, $p<0.05$). This would suggest that an increased hydrophobic area is a key contributor to the inhibition of BFC metabolism. Other QSAR studies have identified some measure of hydrophobicity as key in determining inhibitory potential against CYP3A4, whether it's LogP[13] or the number of aromatic rings or bonds[10,16]. Prior molecular dynamics simulations with CYP3A4 and progesterone indicated several van der Waals contacts between progesterone's steroid core and the side chains of Arg105, Phe108, Ile120, Ile301, and Phe304[27]. Based on these findings, we anticipated descriptors for hydrophobicity to occur more frequently in the TST model due to the role that van der Waals contacts play in progesterone binding. Graphing the distribution of P_VSA_LogP_6 values in the BFC database (Figure 9), both weak and strong inhibitors show reduced surface area with a LogP between 0.2 and 0.25.

Our models would suggest that hydrophobic interactions are of equal or greater importance in BFC metabolism than in TST metabolism. Inhibitors of BFC could form van der Waals contacts with side chains that usually bind with the benzyl ring or coumarin nucleus of BFC.

Comparing the GA-kNN models developed for inhibitors of TST or BFC metabolism by CYP3A4, we found several structural descriptors that differ in importance between models. These findings could be applied to future *in-vitro* CYP3A4 inhibition screens to account for any differences in inhibition with multiple substrates. Similarly, developing and comparing CYP models using different probe substrates would give a more complete understanding of the mechanisms involved in CYP inhibition.

Table 1: Parameters for construction of genetic algorithm-k nearest neighbors.
Parameter values and conditions are listed in the program's command line and the log
files generated by the models.

Modeling parameter	Value	Modeling parameter	Value
Training/test set cutoff	0.5 (for training R^2 and LOO q^2)	**Elitism**	On
# nearest neighbors used	1-9	**Elite individuals ratio**	0.01
Model type	Continuous	**Tournament group size**	3
Neighbor choice and weighting	Minkowski-kind weighting w/ relative squared distances	**Min. diversion**	10^{-3}
Vote sharing	Extra neighbors share votes	**Convergence condition**	10 generations w/ diversion $\leq$ min.
Test set check	R^2 used as check for test set	**Crossover mode**	Uniform
Applicability domain z-cutoff	0.5 (Euclidean distance^2)	**Parent selection**	Tournament
Neighbors in applicability domain	≥ 1	**Crossover/mutaton rate**	0.8/0.7
Unbalanced prediction penalty	0	**Max. generations**	300
Solution size penalty term	0.1	**Population size**	200

Table 2: Mean Values and ANOVA Test Results for Selected Descriptors from BFC and Testosterone Training Sets

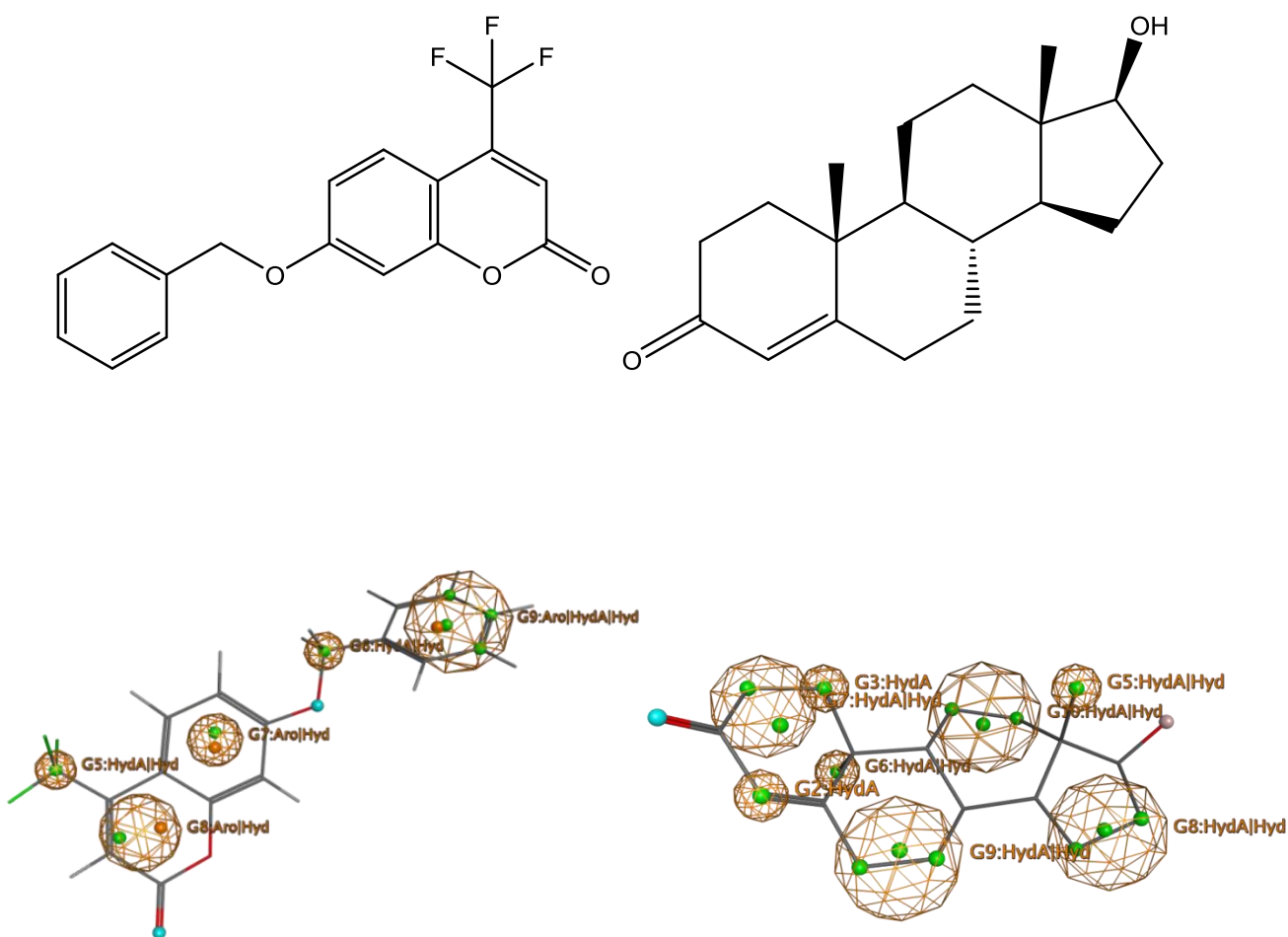|	Descriptor	C-042	NssssC	DLS_cons	nRCONR2	P_VSA_LogP_6	P_VSA_v_3	H-048	H-049	C-033
	BFC mean	0.11	0.78	0.80	0.28	8.09	151.03	0.29	0.38	0.12
	TST mean	0.26	0.54	0.79	0.10	9.95	138.27	0.52	0.99	0.41
ANOVA (single-factor)	F	9.47	5.40	0.31	4.67	1.79	4.37	7.48	28.19	21.04
	P-value	0.00	0.02	0.58	0.03	0.18	0.04	0.01	0.00	0.00

Figure 1: Structures of the probe substrates BFC (left) and testosterone (TST) (right), used to measure CYP3A4 inhibition. Below the line drawings are pharmacophore maps of each structure (created with MOE). Orange globes and green spheres are hydrophobic regions, blue spheres are hydrogen-bond acceptors, and gray spheres act as hydrogen-bond donors and acceptors.
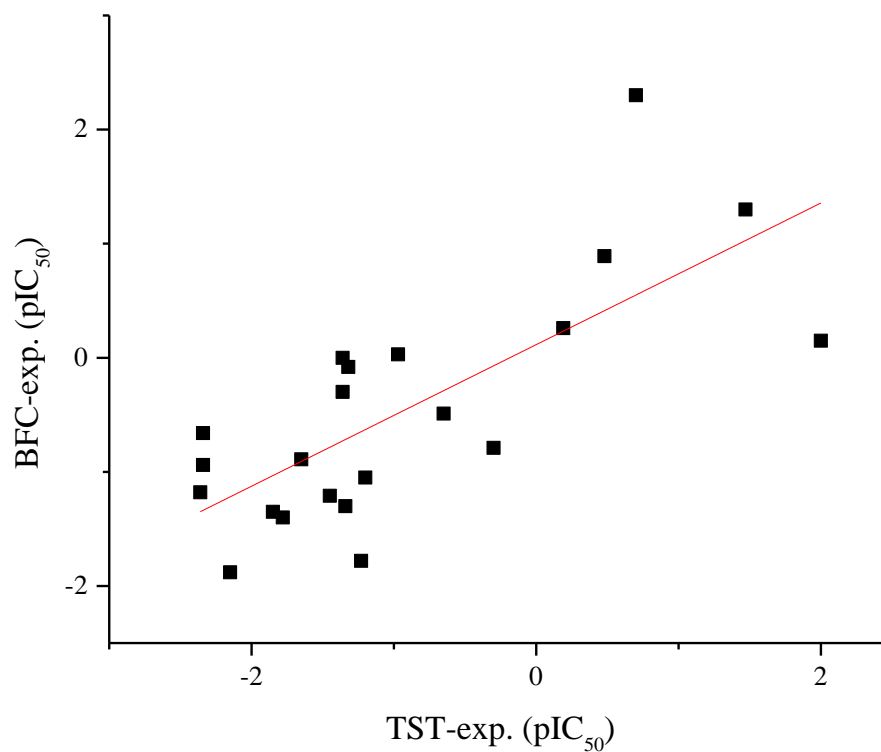
Figure 2: pIC$_{50}$ values of compounds present in both TST and BFC training sets.
The correlation between the activities (R^2=0.52) suggests some common features among
inhibitors, as well as features that make a given compound a more potent inhibitor against
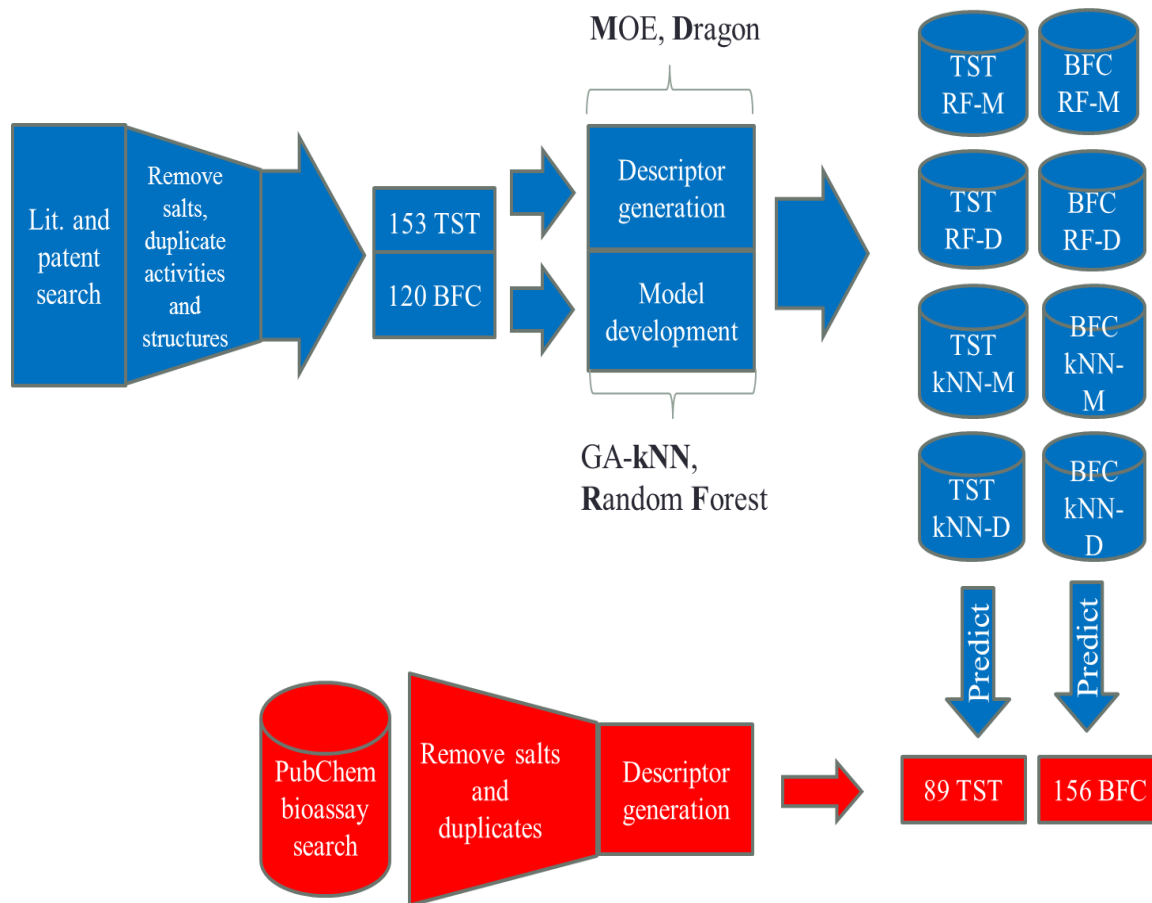CYP3A4 oxidation of one substrate.

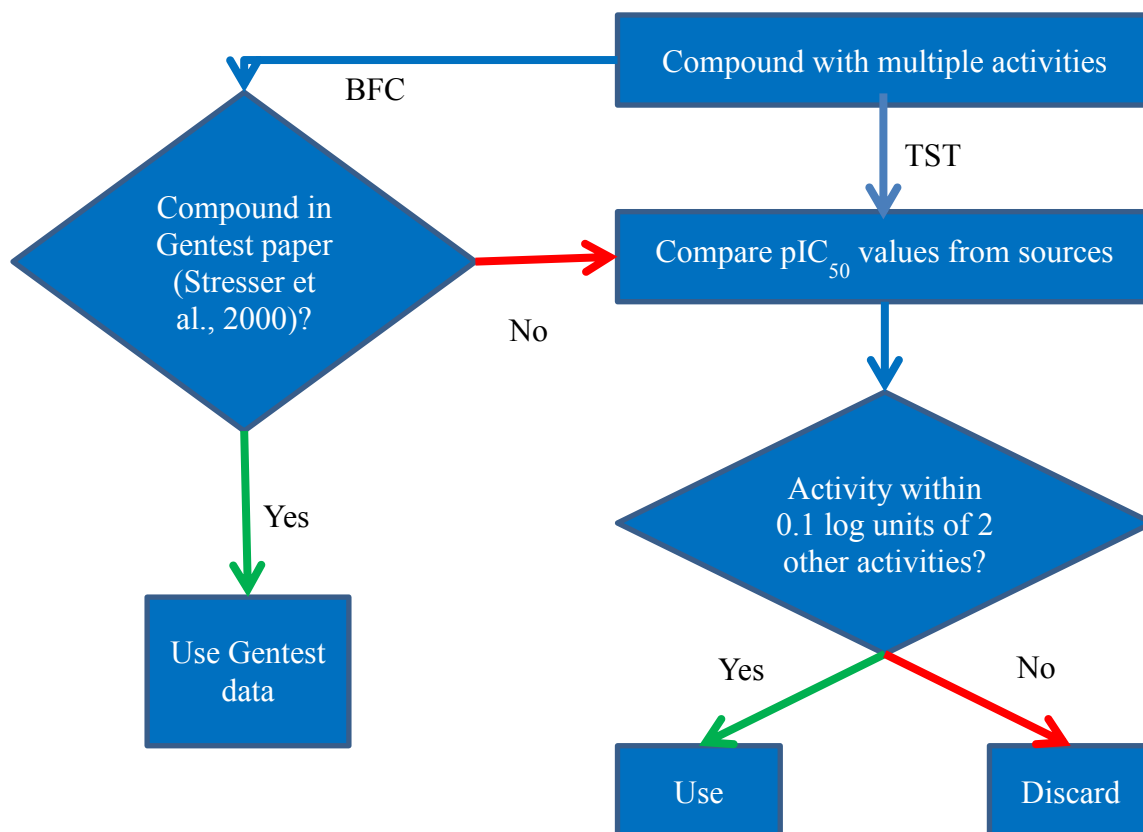**Figure 3: Flowchart for model development and testing**.

Figure 4: Flowchart for Compounds with Duplicate Activities. The Stresser et al. (2000) paper is used as a standard because it is an early study of 7-BFC as a probe substrate, and the authors' parent company (Gentest) is a manufacturer of CYP3A4 inhibition screens that use 7-BFC as a probe substrate.
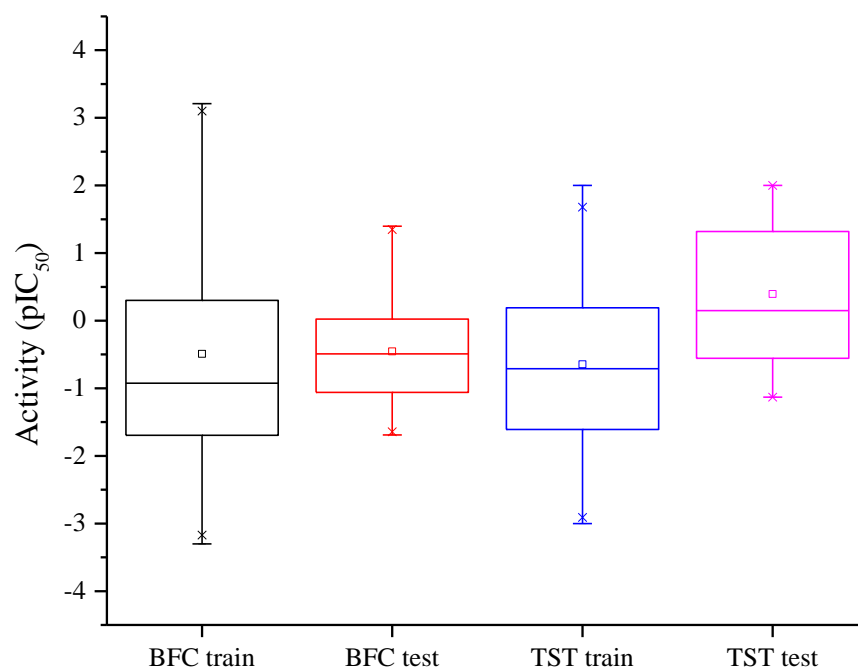
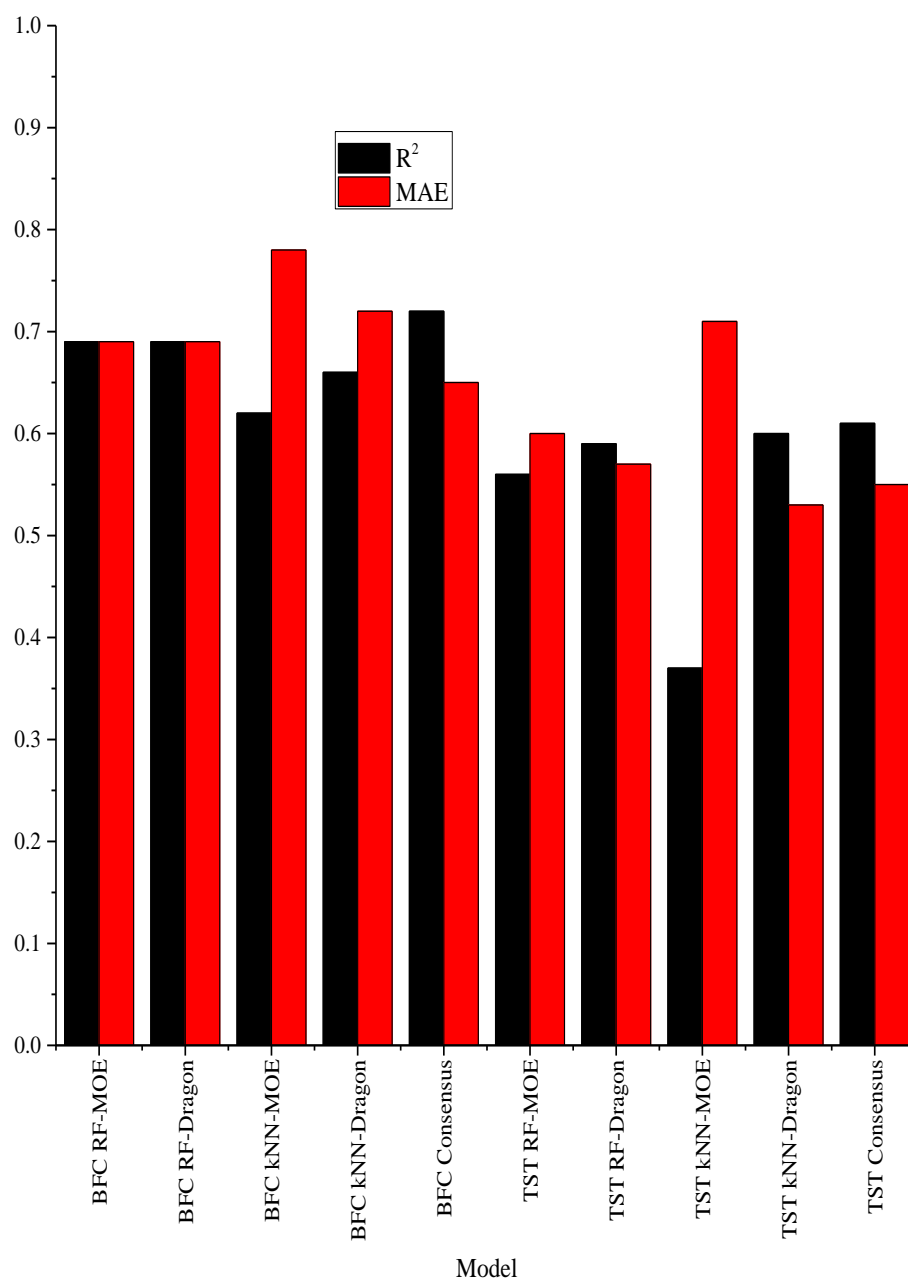**Figure 5: Distribution of activity values in training and test sets**

Figure 6: 5-fold cross-validation results for BFC and TST models. Graph shows correlation coefficient (R^2) and mean absolute error (MAE) for each model. BFC and TST consensus data are obtained by taking the mean of each compound's predicted activity from all BFC or TST models.
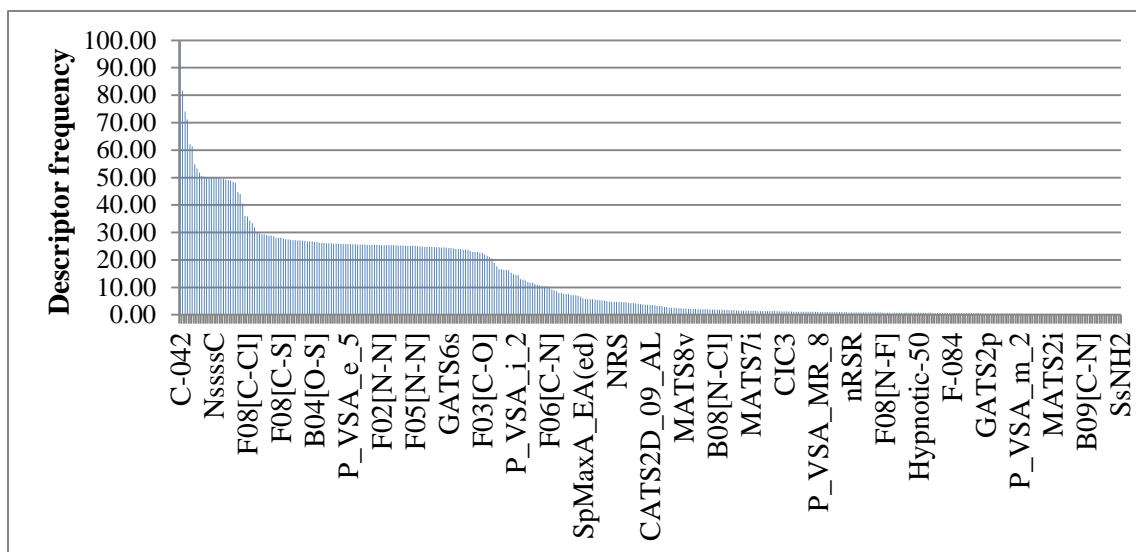
Figure 7: Total importance of all descriptors in BFC and TST Dragon kNN models. For the kNN models, the frequency with which a descriptor appears in a model is used as a proxy measurement for the descriptor's importance. In this graph, descriptor importance is obtained by adding the frequency of each descriptor in the BFC and TST Dragon kNN models.
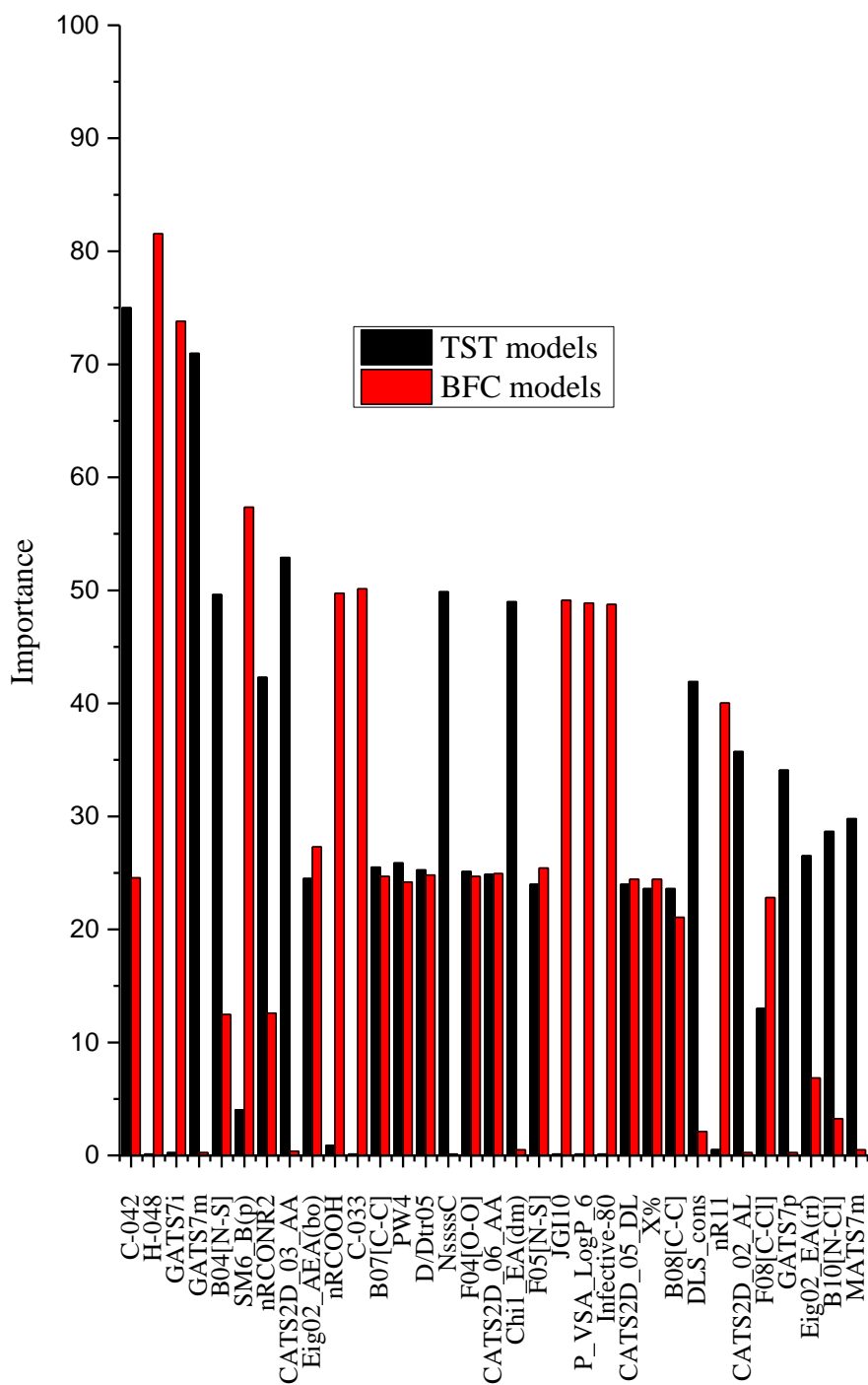
Figure 8: Descriptor importance for selected descriptors in the BFC and TST Dragon kNN models

Figure 9: Distribution of P_VSA_LogP_6 descriptor values in BFC training set

Figure 10: Model performance against test sets, graphed across a range of applicability domains. Graphs are separated by probe substrate and descriptor set. Each individual graph measures the R^2 and MAE values for the kNN and RF models. The z-value determines the size of the applicability domain, with coverage directly correlated.

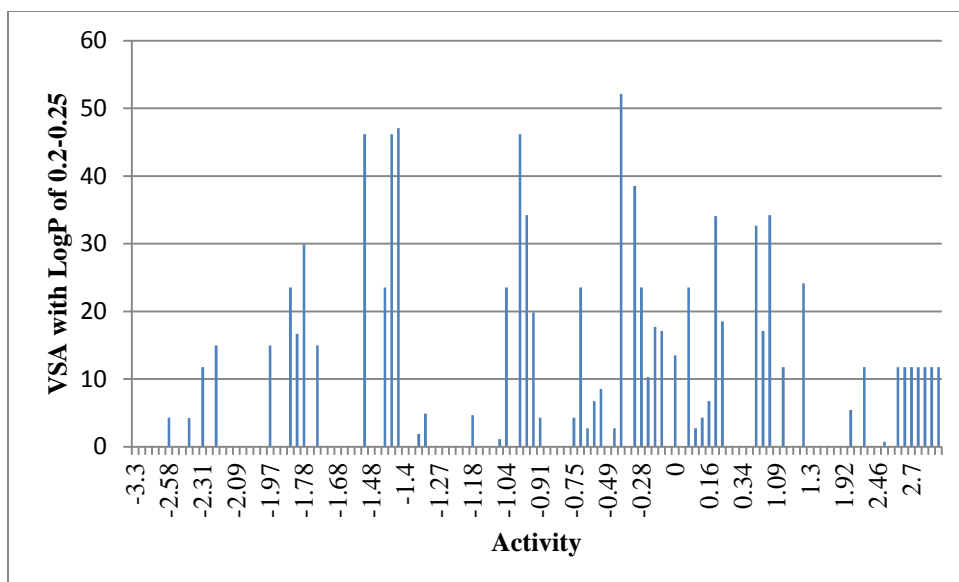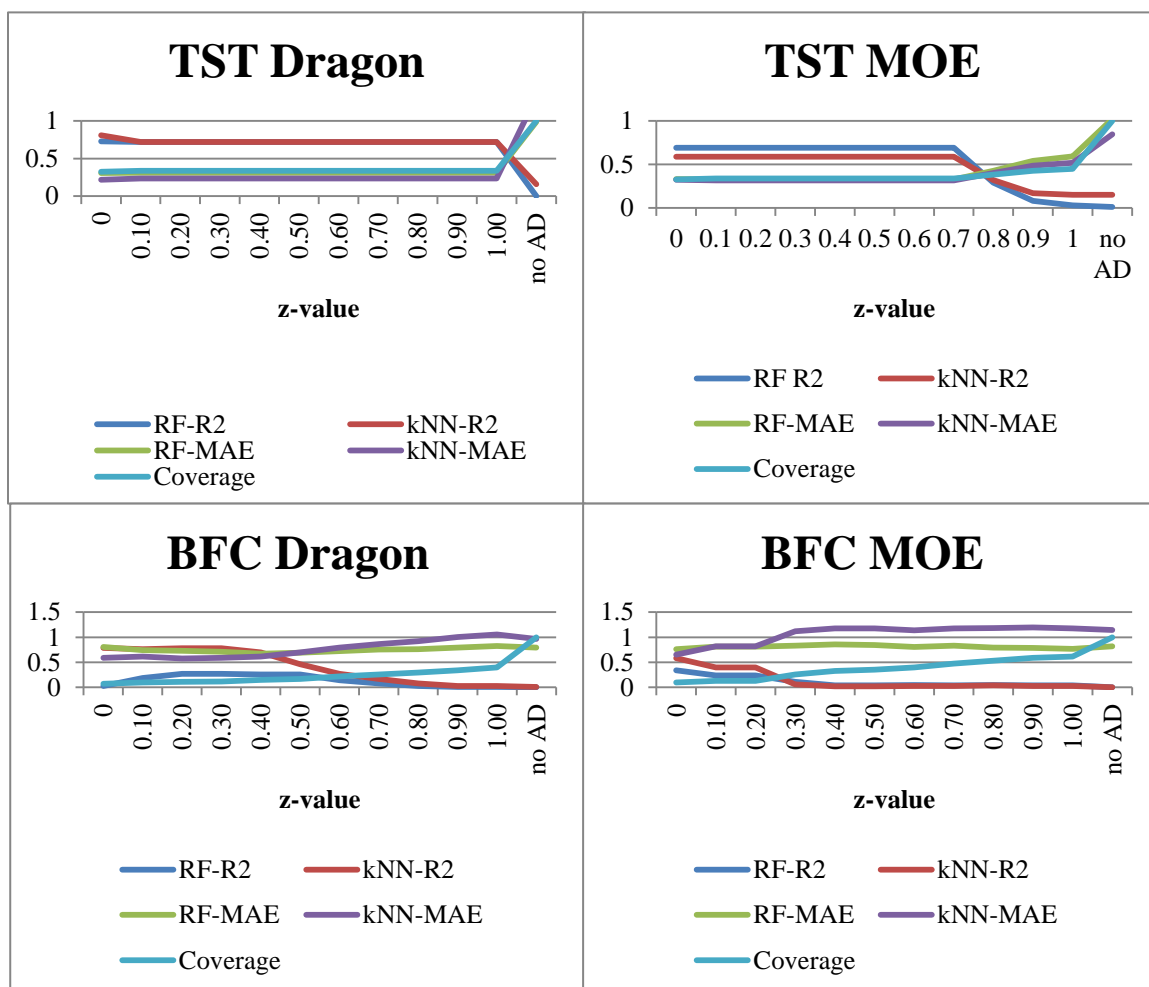APPENDIX 1: Literature and Patent Sources for Training Compounds

1.   Asano, T. *et al.* Metabolism of ipecac alkaloids cephaeline and emetine by human hepatic microsomal cytochrome P450s, and their inhibitory effects on P450 enzyme activities. *Biol. Pharm. Bull.* **24,** 678–82 (2001).

2.   Badal, S. *et al.* Cytochrome P450 1 enzyme inhibition and anticancer potential of chromene amides from Amyris plumieri. *Fitoterapia* **82,** 230–6 (2011).

3.   Bapiro, T. E., Egnell, A., Hasler, J. A. & Masimirembwa, C. M. APPLICATION OF HIGHER THROUGHPUT SCREENING (HTS) INHIBITION ASSAYS TO EVALUATE THE INTERACTION OF ANTIPARASITIC DRUGS WITH CYTOCHROME P450S. *Drug Metab. Dispos.* **29,** 30–35 (2001).

4.   Bell, L. *et al.* Evaluation of fluorescence- and mass spectrometry-based CYP inhibition assays for use in drug discovery. *J. Biomol. Screen.* **13,** 343–53 (2008).

5.   Brahmi, Z. *et al.* Effective Cytochrome P450 (CYP) Inhibitor Isolated from Thyme (Thymus saturoides) Purchased from a Japanese Market. *Biosci. Biotechnol. Biochem.* **75,** 2237–2239 (2011).

6.   Cai, Z.-W. *et al.* Synthesis, SAR, and Evaluation of 4-[2,4-Difluoro-5-(cyclopropylcarbamoyl)phenylamino]pyrrolo[2,1-f][1,2,4]triazine-based VEGFR-2 kinase inhibitors. *Bioorg. Med. Chem. Lett.* **18,** 1354–8 (2008).

7.   Chiba, M. *et al.* P450 interaction with farnesyl-protein transferase inhibitors metabolic stability, inhibitory potency, and P450 binding spectra in human liver microsomes. *Biochem. Pharmacol.* **62,** 773–6 (2001).

8.   Chiba, M., Hensleigh, M., Nishime, J. A., Balani, S. K. & Lin, J. H. Role of cytochrome P450 3A4 in human metabolism of MK-639, a potent Human Immunodeficiency Virus protease inhibitor. *Drug Metab. Dispos.* **24,** 307–314 (1996).

9.   Chiba, M. *et al.* P450 Interaction with HIV Protease Inhibitors: Relationship between Metabolic Stability, Inhibitory Potency, and P450 Binding Spectra. *Drug Metab. Dispos.* **29,** 1–3 (2001).

10.   Choi, D.-H., Li, C. & Choi, J.-S. Effects of myricetin, an antioxidant, on the pharmacokinetics of losartan and its active metabolite, EXP-3174, in rats: possible role of cytochrome P450 3A4, cytochrome P450 2C9 and P-glycoprotein inhibition by myricetin. *J. Pharm. Pharmacol.* **62,** 908–14 (2010).

11.   Cohen, L. H., van Leeuwen, R. E., van Thiel, G. C., van Pelt, J. F. & Yap, S. H. Equally potent inhibitors of cholesterol synthesis in human hepatocytes have

distinguishable effects on different cytochrome P450 enzymes. *Biopharm. Drug Dispos.* **21,** 353–64 (2000).

12. Corminboeuf, O. *et al.* Design and optimization of new piperidines as renin inhibitors. *Bioorg. Med. Chem. Lett.* **20,** 6286–90 (2010).

13. Crespi, C. L., Miller, V. P. & Penman, B. W. Microtiter Plate Assays for Inhibition of Human, Drug-Metabolizing Cytochromes P450. *Anal. Biochem.* **248,** 188–190 (1997).

14. Denton, T. T., Zhang, X. & Cashman, J. R. Analogues of Nicotine as Selective Inhibitors of Cytochrome P-450 2A6. *J. Med. Chem.* **48,** 224–239 (2005).

15. Duffy, J. L. *et al.* HIV-1 protease inhibitors with picomolar potency against PI-resistant HIV-1 by modification of the P1′ substituent. *Bioorg. Med. Chem. Lett.* **13,** 3323–3326 (2003).

16. Eagling, V. a, Back, D. J. & Barry, M. G. Differential inhibition of cytochrome P450 isoforms by the protease inhibitors, ritonavir, saquinavir and indinavir. *Br. J. Clin. Pharmacol.* **44,** 190–4 (1997).

17. Flentge, C. a *et al.* Synthesis and evaluation of inhibitors of cytochrome P450 3A (CYP3A) for pharmacokinetic enhancement of drugs. *Bioorg. Med. Chem. Lett.* **19,** 5444–8 (2009).

18. Ganzera, M., Schneider, P. & Stuppner, H. Inhibitory effects of the essential oil of chamomile (Matricaria recutita L.) and its major constituents on human cytochrome P450 enzymes. *Life Sci.* **78,** 856–61 (2006).

19. Girennavar, B., Jayaprakasha, G. K. & Patil, B. S. Potent inhibition of human cytochrome P450 3A4, 2D6, and 2C9 isoenzymes by grapefruit juice and its furocoumarins. *J. Food Sci.* **72,** C417–21 (2007).

20. Girennavar, B., Jayaprakasha, G. K., Jadegoud, Y., Nagana Gowda, G. a & Patil, B. S. Radical scavenging and cytochrome P450 3A4 inhibitory activity of bergaptol and geranylcoumarin from grapefruit. *Bioorg. Med. Chem.* **15,** 3684–91 (2007).

21. Holsworth, D. D. *et al.* Ketopiperazine-based renin inhibitors: optimization of the "C" ring. *Bioorg. Med. Chem. Lett.* **16,** 2500–4 (2006).

22. Isoherranen, N., Kunze, K. L., Allen, K. E., Nelson, W. L. & Thummel, K. E. ROLE OF ITRACONAZOLE METABOLITES IN CYP3A4 INHIBITION. *Drug Metab. Dispos.* **32,** 1121–1131 (2004).

23.   Jeong, S., Nguyen, P. D. & Desta, Z. Comprehensive in vitro analysis of voriconazole inhibition of eight cytochrome P450 (CYP) enzymes: major effect on CYPs 2B6, 2C9, 2C19, and 3A. *Antimicrob. Agents Chemother.* **53,** 541–51 (2009).

24.   Kaku, T. *et al.* 17,20-Lyase inhibitors. Part 3: Design, synthesis, and structure-activity relationships of biphenylylmethylimidazole derivatives as novel 17,20-lyase inhibitors. *Bioorg. Med. Chem.* **19,** 2428–42 (2011).

25.   Karonen, T., Neuvonen, P. J. & Backman, J. T. CYP2C8 but not CYP3A4 is important in the pharmacokinetics of montelukast. *Br. J. Clin. Pharmacol.* **73,** 257–67 (2012).

26.   Kharasch, E. D., Bedynek, P. S., Hoffer, C., Walker, A. & Whittington, D. Lack of indinavir effects on methadone disposition despite inhibition of hepatic and intestinal cytochrome P4503A (CYP3A). *Anesthesiology* **116,** 432–47 (2012).

27.   Kimura, Y., Ito, H., Ohnishi, R. & Hatano, T. Inhibitory effects of polyphenols on human cytochrome P450 3A4 and 2C9 activity. *Food Chem. Toxicol.* **48,** 429–35 (2010).

28.   Kraus, J. M. *et al.* Second generation analogues of the cancer drug clinical candidate tipifarnib for anti-Chagas disease drug discovery. *J. Med. Chem.* **53,** 3887–98 (2010).

29.   Kumar, S. & Kumar, A. Differential effects of ethanol on spectral binding and inhibition of cytochrome P450 3A4 with eight protease inhibitors antiretroviral drugs. *Alcohol. Clin. Exp. Res.* **35,** 2121–7 (2011).

30.   Lee, J. Y., Kang, N. S. & Kang, Y. K. Binding free energies of inhibitors to iron porphyrin complex as a model for Cytochrome P450. *Biopolymers* **97,** 219–28 (2012).

31.   Lee, J., Duke, R. K., Tran, V. H., Hook, J. M. & Duke, C. C. Hyperforin and its analogues inhibit CYP3A4 enzyme activity. *Phytochemistry* **67,** 2550–60 (2006).

32.   Li, Y., Sundermann, K., Tang, L. & Myles, D. Trans-9,10-dehydroepothilone C and D, analogs thereof and methods of making the same. WO 2004/043954 A2 (2004).

33.   Liu, Y., Ma, H., Zhang, J.-W., Deng, M.-C. & Yang, L. Influence of ginsenoside Rh1 and F1 on human cytochrome p450 enzymes. *Planta Med.* **72,** 126–31 (2006).

34.   Mar, J. *et al.* IN SILICO AND IN VITRO SCREENING FOR INHIBITION OF CYTOCHROME P450 CYP3A4 BY COMEDICATIONS COMMONLY USED BY PATIENTS WITH CANCER. *Drug Metab. Dispos.* **34,** 534–538 (2006).

35.   Nath, A., Zientek, M. A., Burke, B. J., Jiang, Y. & Atkins, W. M. Quantifying and Predicting the Promiscuity and Isoform Specificity of Small-Molecule Cytochrome P450 Inhibitors. *Drug Metab. Dispos.* **38,** 2195–2203 (2010).

36.   Nicolas, J. M., Whomsley, R., Collart, P. & Roba, J. In vitro inhibition of human liver drug metabolizing enzymes by second generation antihistamines. *Chem. Biol. Interact.* **123,** 63–79 (1999).

37.   Obach, R. S. Inhibition of Human Cytochrome P450 Enzymes by Constituents of St . John ' s Wort , an Herbal Preparation Used in the Treatment of Depression. *J. Pharmacol. Exp. Ther.* **294,** 88–95 (2000).

38.   Park, J., Kim, K. & Kim, S. Chloramphenicol Is a Potent Inhibitor of Cytochrome P450 Isoforms CYP2C19 and CYP3A4 in Human Liver Microsomes. *Antimicrob. Agents Chemother.* **47,** 3464–3469 (2003).

39.   Patel, C. G. *et al.* Two-way pharmacokinetic interaction studies between saxagliptin and cytochrome P450 substrates or inhibitors: simvastatin, diltiazem extended-release, and ketoconazole. *Clin. Pharmacol.* **3,** 13–25 (2011).

40.   Patterson, B., Sakata, S., Nambu, M., Patel, L. & Tatlock, J. Therapeutic compounds. WO2007034312A2 (2007).

41.   Poulose, S. M., Jayaprakasha, G. K., Mayer, R. T., Girennavar, B. & Patil, B. S. Purification of citrus limonoids and their differential inhibitory effects on human cytochrome P450 enzymes. *J. Sci. Food Agric.* **1709,** 1699–1709 (2007).

42.   Riley, R. J., Parker, a J., Trigg, S. & Manners, C. N. Development of a generalized, quantitative physicochemical model of CYP3A4 inhibition for use in early drug discovery. *Pharm. Res.* **18,** 652–5 (2001).

43.   Row, E. C., Brown, S. a, Stachulski, a V & Lennard, M. S. Synthesis of 8-geranyloxypsoralen analogues and their evaluation as inhibitors of CYP3A4. *Bioorg. Med. Chem.* **14,** 3865–71 (2006).

44.   Row, E. C., Brown, S. a, Stachulski, a V & Lennard, M. S. Design, synthesis and evaluation of furanocoumarin monomers as inhibitors of CYP3A4. *Org. Biomol. Chem.* **4,** 1604–10 (2006).

45.   Row, E. *et al.* DEVELOPMENT OF NOVEL FURANOCOUMARIN DIMERS AS POTENT AND SELECTIVE INHIBITORS OF CYP3A4. *Drug Metab. Dispos.* **34,** 324–330 (2006).

46.   Sai, Y. *et al.* Assessment of specificity of eight chemical inhibitors using cDNA-expressed cytochromes P450. *Xenobiotica* **30,** 327–343 (2000).

47.   Sakaeda, T. *et al.* Effects of acid and lactone forms of eight HMG-CoA reductase inhibitors on CYP-mediated metabolism and MDR1-mediated transport. *Pharm. Res.* **23,** 506–12 (2006).

48.   Schwab, D., Fischer, H., Tabatabaei, A., Poli, S. & Huwyler, J. Comparison of in vitro P-glycoprotein screening assays: recommendations for their use in drug discovery. *J. Med. Chem.* **46,** 1716–25 (2003).

49.   Sekiguchi, N. *et al.* Prediction of Drug-Drug Interactions based on Time-Dependent Inhibition from High Throughput Screening of Cytochrome P450 3A4 Inhibition. *Drug Metab. Pharmacokinet.* **24,** 500–510 (2009).

50.   Shi, Y. *et al.* Aroylguanidine-based factor Xa inhibitors: the discovery of BMS-344577. *Bioorg. Med. Chem. Lett.* **19,** 6882–9 (2009).

51.   Shimada, T. *et al.* Structure-function relationships of inhibition of human cytochromes P450 1A1, 1A2, 1B1, 2C9, and 3A4 by 33 flavonoid derivatives. *Chem. Res. Toxicol.* **23,** 1921–35 (2010).

52.   Stresser, D. M., Blanchard, A. P., Miller, V. P. & Crespi, C. L. GENTEST Corp.-SUBSTRATE DEPENDENT EFFECTS ON CYP3A4 INHIBITION OR ACTIVATION BY 20 TEST COMPOUNDS. **4,** 1 (1998).

53.   Stresser, D. M. *et al.* SUBSTRATE-DEPENDENT MODULATION OF CYP3A4 CATALYTIC ACTIVITY : ANALYSIS OF 27 TEST COMPOUNDS WITH FOUR FLUOROMETRIC SUBSTRATES. *Drug Metab. Dispos.* **28,** 1440–1448 (2000).

54.   Su, C.-R., Ueng, Y.-F., Dung, N. X., Vijaya Bhaskar Reddy, M. & Wu, T.-S. Cytochrome P3A4 inhibitors and other constituents of Fibraurea tinctoria. *J. Nat. Prod.* **70,** 1930–3 (2007).

55.   Subehan, Zaidi, S. F. H., Kadota, S. & Tezuka, Y. Inhibition on human liver cytochrome P450 3A4 by constituents of fennel (Foeniculum vulgare): identification and characterization of a mechanism-based inactivator. *J. Agric. Food Chem.* **55,** 10162–7 (2007).

56.   Velaparthi, U. *et al.* Insulin-like growth factor-1 receptor (IGF-1R) kinase inhibitors: SAR of a series of 3-[6-(4-substituted-piperazin-1-yl)-4-methyl-1H-benzimidazol-2-yl]-1H-pyridine-2-one. *Bioorg. Med. Chem. Lett.* **20,** 3182–5 (2010).

57.   Wanchana, S., Yamashita, F. & Hashida, M. QSAR analysis of the inhibition of recombinant CYP 3A4 activity by structurally diverse compounds using a genetic algorithm-combined partial least squares method. *Pharm. Res.* **20,** 1401–8 (2003).

58. Winitthana, T., Niwattisaiwong, N., Patarapanich, C., Tantisira, M. H. & Lawanprasert, S. In vitro inhibitory effects of asiaticoside and madecassoside on human cytochrome P450. *Toxicol. In Vitro* **25,** 890–6 (2011).

59. Xie, Z., Zhang, T., Wang, J.-F., Chou, K.-C. & Wei, D.-Q. The computational model to predict accurately inhibitory activity for inhibitors towards CYP3A4. *Comput. Biol. Med.* **40,** 845–52 (2010).

60. Young, J. R. *et al.* Pyrrolidine-carboxamides and oxadiazoles as potent hNK1 antagonists. *Bioorg. Med. Chem. Lett.* **17,** 5310–5 (2007).

61. Zhao, T. *et al.* Inhibition of human cytochrome P450 enzymes 3A4 and 2D6 by β-carboline alkaloids, harmine derivatives. *Phytother. Res.* **25,** 1671–7 (2011).

62. Zimmerlin, A., Trunzer, M. & Faller, B. CYP3A Time-Dependent Inhibition Risk Assessment Validated with 400 Reference Drugs. *Drug Metab. Dispos.* **39,** 1039–1046 (2011).

APPENDIX 2: Literature Sources for Testing Compounds

1. Adams, C. M. *et al.* The discovery of potent inhibitors of aldosterone synthase that exhibit selectivity over 11-beta-hydroxylase. *Bioorg. Med. Chem. Lett.* **20,** 4324–7 (2010).

2. Ahlström, M. M. & Zamora, I. Characterization of type II ligands in CYP2C9 and CYP3A4. *J. Med. Chem.* **51,** 1755–63 (2008).

3. Aspiotis, R. *et al.* The discovery and synthesis of potent zwitterionic inhibitors of renin. *Bioorg. Med. Chem. Lett.* **21,** 2430–6 (2011).

4. Berglund, S. *et al.* Optimization of piperidin-4-yl-urea-containing melanin-concentrating hormone receptor 1 (MCH-R1) antagonists: Reducing hERG-associated liabilities. *Bioorg. Med. Chem. Lett.* **19,** 4274–9 (2009).

5. Cai, Z.-W. *et al.* Synthesis, SAR, and Evaluation of 4-[2,4-Difluoro-5-(cyclopropylcarbamoyl)phenylamino]pyrrolo[2,1-f][1,2,4]triazine-based VEGFR-2 kinase inhibitors. *Bioorg. Med. Chem. Lett.* **18,** 1354–8 (2008).

6. Holsworth, D. D. *et al.* Ketopiperazine-based renin inhibitors: optimization of the "C" ring. *Bioorg. Med. Chem. Lett.* **16,** 2500–4 (2006).

7. Kaku, T. *et al.* 17,20-lyase inhibitors. Part 4: design, synthesis and structure-activity relationships of naphthylmethylimidazole derivatives as novel 17,20-lyase inhibitors. *Bioorg. Med. Chem.* **19,** 1751–70 (2011).

8. Kaku, T. *et al.* 17,20-Lyase inhibitors. Part 3: Design, synthesis, and structure-activity relationships of biphenylylmethylimidazole derivatives as novel 17,20-lyase inhibitors. *Bioorg. Med. Chem.* **19,** 2428–42 (2011).

9. Koltun, E. *et al.* Discovery of a new class of glucosylceramide synthase inhibitors. *Bioorg. Med. Chem. Lett.* **21,** 6773–7 (2011).

10. Kraus, J. M. *et al.* Rational modification of a candidate cancer drug for use against Chagas disease. *J. Med. Chem.* **52,** 1639–47 (2009).

11. Labrie, P. *et al.* In vitro activity of novel dual action MDR anthranilamide modulators with inhibitory activity on CYP-450 (Part 2). *Bioorg. Med. Chem.* **15,** 3854–68 (2007).

12. Martyn, D. C. *et al.* Synthesis and in vitro DMPK profiling of a 1,2-dioxolane-based library with activity against Plasmodium falciparum. *Bioorg. Med. Chem. Lett.* **19,** 5657–60 (2009).

13. Min, K. H. *et al.* A novel class of highly potent multidrug resistance reversal agents: disubstituted adamantyl derivatives. *Bioorg. Med. Chem. Lett.* **19,** 5376–9 (2009).

14. Ohnmacht, S., Nava, P., West, R., Parker, R. & Atkinson, J. Inhibition of oxidative metabolism of tocopherols with omega-N-heterocyclic derivatives of vitamin E. *Bioorg. Med. Chem.* **16,** 7631–8 (2008).

15. Velaparthi, U. *et al.* Discovery and Evaluation of 4- (2- (4-chloro- 1 H -pyrazol-1-yl) ethylamino) -3- (6- (1- (3-fluoro- propyl) piperidin-4-yl) -4-methyl-1 H -benzo [d] imidazol-2-yl) pyridin-2 (1 H) -one (BMS-695735), an Orally Efficacious Inhibitor of Insu. 5897–5900 (2008).

16. Vrudhula, V. M. *et al.* Analogs of a potent maxi-K potassium channel opener with an improved inhibitory profile toward cytochrome P450 isozymes. *Bioorg. Med. Chem. Lett.* **15,** 4286–90 (2005).

17. Yano, J. K. *et al.* Synthetic inhibitors of cytochrome P-450 2A6: inhibitory activity, difference spectra, mechanism of inhibition, and protein cocrystallization. *J. Med. Chem.* **49,** 6987–7001 (2006).

18. Zehnder, L. *et al.* Optimization of Potent , Selective , and Orally Bioavailable Pyrrolodinopyrimidine-Containing Inhibitors of Heat Shock Protein 90 . Identification of Development Candidate. **14,** 3368–3385 (2011).

19. Zhang, X. *et al.* Lead Optimization of 4-Acetylamino-2- (3 , 5-dimethylpyrazol-1-yl) -6-pyridylpyrimidines as A 2A Adenosine Receptor Antagonists for the Treatment of Parkinson ' s Disease. **1,** 7099–7110 (2008).

REFERENCES

1.   Guengerich, F. P. Cytochrome p450 and chemical toxicology. *Chem. Res. Toxicol.* **21,** 70–83 (2008).

2.   Moroy, G., Martiny, V. Y., Vayer, P., Villoutreix, B. O. & Miteva, M. a. Toward in silico structure-based ADMET prediction in drug discovery. *Drug Discov. Today* **17,** 44–55 (2012).

3.   Singh, S. B., Shen, L. Q., Walker, M. J. & Sheridan, R. P. A model for predicting likely sites of CYP3A4-mediated metabolism on drug-like molecules. *J. Med. Chem.* **46,** 1330–6 (2003).

4.   Yano, J. K. *et al.* The structure of human microsomal cytochrome P450 3A4 determined by X-ray crystallography to 2.05-A resolution. *J. Biol. Chem.* **279,** 38091–4 (2004).

5.   Galetin, A., Clarke, S. E. & Houston, J. B. MULTISITE KINETIC ANALYSIS OF INTERACTIONS BETWEEN PROTOTYPICAL CYP3A4 SUBGROUP SUBSTRATES : MIDAZOLAM , TESTOSTERONE , AND NIFEDIPINE. *Drug Metab. Dispos.* **31,** 1108–1116 (2003).

6.   Lu, P. *et al.* TRIFLUOROMETHYL-COUMARIN BIND TO DIFFERENT DOMAINS WITHIN THE ACTIVE SITE OF CYTOCHROME P450 3A4 ABSTRACT : **29,** 1473–1479 (2001).

7.   Domanski, T. L. *et al.* Phenylalanine and tryptophan scanning mutagenesis of CYP3A4 substrate recognition site residues and effect on substrate oxidation and cooperativity. *Biochemistry* **40,** 10150–60 (2001).

8.   Schrag, M. L. & Wienkers, L. C. Covalent alteration of the CYP3A4 active site: evidence for multiple substrate binding domains. *Arch. Biochem. Biophys.* **391,** 49–55 (2001).

9.   Shimada, T. *et al.* Structure-function relationships of inhibition of human cytochromes P450 1A1, 1A2, 1B1, 2C9, and 3A4 by 33 flavonoid derivatives. *Chem. Res. Toxicol.* **23,** 1921–35 (2010).

10.   Sun, H., Veith, H., Xia, M., Austin, C. P. & Huang, R. Predictive models for cytochrome p450 isozymes based on quantitative high throughput screening data. *J. Chem. Inf. Model.* **51,** 2474–81 (2011).

11.   Ekins, S. *et al.* Three- and four-dimensional quantitative structure activity relationship analyses of cytochrome P-450 3A4 inhibitors. *J. Pharmacol. Exp. Ther.* **290,** 429–38 (1999).

12. Row, E. *et al.* DEVELOPMENT OF NOVEL FURANOCOUMARIN DIMERS AS POTENT AND SELECTIVE INHIBITORS OF CYP3A4. *Drug Metab. Dispos.* **34,** 324–330 (2006).

13. Kriegl, J. M. *et al.* Multivariate modeling of cytochrome P450 3A4 inhibition. *Eur. J. Pharm. Sci.* **24,** 451–63 (2005).

14. Roy, K. & Pratim Roy, P. Comparative chemometric modeling of cytochrome 3A4 inhibitory activity of structurally diverse compounds using stepwise MLR, FA-MLR, PLS, GFA, G/PLS and ANN techniques. *Eur. J. Med. Chem.* **44,** 2913–22 (2009).

15. Riley, R. J., Parker, a J., Trigg, S. & Manners, C. N. Development of a generalized, quantitative physicochemical model of CYP3A4 inhibition for use in early drug discovery. *Pharm. Res.* **18,** 652–5 (2001).

16. Zuegge, J. *et al.* A fast virtual screening filter for cytochrome P450 3A4 inhibition liability of compound libraries. *Quant. Struct. Relationships* **21,** 249–256 (2002).

17. Ekroos, M. & Sjögren, T. Structural basis for ligand promiscuity in cytochrome P450 3A4. *Proc. Natl. Acad. Sci. U. S. A.* **103,** 13682–7 (2006).

18. Mao, B. *et al.* QSAR modeling of in vitro inhibition of cytochrome P450 3A4. *J. Chem. Inf. Model.* **46,** 2125–34 (2006).

19. Stresser, D. M. *et al.* SUBSTRATE-DEPENDENT MODULATION OF CYP3A4 CATALYTIC ACTIVITY : ANALYSIS OF 27 TEST COMPOUNDS WITH FOUR FLUOROMETRIC SUBSTRATES. *Drug Metab. Dispos.* **28,** 1440–1448 (2000).

20. Zheng, W. & Tropsha, a. Novel variable selection quantitative structure--property relationship approach based on the k-nearest-neighbor principle. *J. Chem. Inf. Comput. Sci.* **40,** 185–94 (2000).

21. Tropsha, A. & Golbraikh, A. Predictive QSAR modeling workflow, model applicability domains, and virtual screening. *Curr. Pharm. Des.* **13,** 3494–504 (2007).

22. Golbraikh, A. *et al.* Rational selection of training and test sets for the development of validated QSAR models. *J. Comput. Aided. Mol. Des.* **17,** 241–53 (2003).

23. Breiman, L. E. O. Random Forests. 5–32 (2001).

24. Viswanadhan, V. N., Ghose, A. K., Reyankar, G. R., Robins, R. K. & Al, E. T. Atomic Physicochemical Parameters for Three Dimensional Structure Directed Quantitative Structure-Activity Relationships . 4 . Additional Parameters for

Hydrophobic and Dispersive Interactions and Their Application for an Automated Superposition of Certai. *J. Cheminformatics Comput. Sci.* **29,** 163–172 (1989).

25. Row, E. C., Brown, S. a, Stachulski, a V & Lennard, M. S. Design, synthesis and evaluation of furanocoumarin monomers as inhibitors of CYP3A4. *Org. Biomol. Chem.* **4,** 1604–10 (2006).

26. Labute, P. A widely applicable set of descriptors. *J. Mol. Graph. Model.* **18,** 464–77 (2000).

27. Park, H., Lee, S. & Suh, J. Structural and dynamical basis of broad substrate specificity, catalytic mechanism, and inhibition of cytochrome P450 3A4. *J. Am. Chem. Soc.* **127,** 13634–42 (2005).

28. D. E. Goldberg, *Genetic Algorithms in Search, Optimization, and Machine Learning*, Addison-Wesley, Boston, Massachusetts, 1989.